IOP Publishing Journal of Physics D: Applied Physics

J. Phys. D: Appl. Phys. **48** (2015) 455201 (16pp) doi:10.1088/0022-3727/48/45/455201

Achieving an intense enough maintenance electric field in a low-pressure discharge sustained by a microwave field under ambipolar diffusion regime such that periodic parametric instabilities are generated[3]

M Moisan[1] and H Nowakowska[2]

[1] Groupe de physique des plasmas, Université de Montréal, Montréal H3C 3J7, Québec
[2] Centre for Plasma and Laser Engineering, The Szewalski Institute of Fluid-Flow Machinery, Polish Academy of Sciences, 80-952 Gdansk, Poland

E-mail: michel.moisan@umontreal.ca

Received 18 March 2015, revised 27 May 2015
Accepted for publication 24 July 2015
Published 8 October 2015

Abstract

The intensity of the maintenance electric field of a given discharge is one of its internal parameters. Under ambipolar diffusion conditions, it is almost exclusively set by particle losses, which are related to the dimensions of the discharge vessel and to the gas pressure, and ultimately are determined by the electron energy distribution function. For instance, raising the density of microwave power absorbed in a discharge tube essentially increases the electron density without much increasing the amplitude of the maintenance E-field. To raise the intensity of this E-field in such a case, one needs to reduce the volume into which electromagnetic power is absorbed relative to the diffusion volume, i.e. the volume within which electrons transfer their power through collisions with heavy particles.

To show this point, we consider a power balance based on the power lost per electron through collisions with heavy particles, θ_L, to the power absorbed (over a period of the microwave field) per electron in the discharge, θ_A. The power θ_A, which depends on E_0^2, the square of the amplitude (intensity) of the maintenance electric field, adjusts to compensate for the power lost θ_L. The analysis presented is achieved for a particular microwave discharge configuration that is known to provide an intense E_0-field, which means $x \geqslant \lambda_{De}$, where x is the oscillation amplitude of electrons in the E_0-field and λ_{De} the electron Debye length. Such a condition allows one to observe periodic parametric instabilities at, or close to, the electron-plasma frequency f_{pe} and at their corresponding ion-plasma frequency f_{pi}, these oscillations being caused by the simultaneous propagation of an electron-plasma wave and an ion-plasma wave in the discharge as a result of an applied 'pump' power, which also sustains the discharge.

A 2D hydrodynamic calculation of the specific plasma discharge system is performed, which yields the value of the x/λ_{De} ratio in particular through a global energy balance equation. This equation requires that the volume over which power is absorbed in the discharge multiplied by θ_A must be equal to the discharge diffusion volume multiplied by θ_L, to which must be added the power lost in the ambipolar field E_a and in the plasma sheath.

[3] This paper is dedicated to the memory of Prof Z Zakrzewski (1935–2014), a microwave discharge specialist.

By comparison, in electromagnetic surface-wave discharges these two volumes are equal. The present considerations could possibly be extended to obtain a better insight into dc, RF and microwave micro-discharges when their discharge volume appears to be smaller than the volume over which particles are lost. Such a situation could explain their unusually high level of absorbed power density, as a result of which highly excited and ionized plasmas are generated.

Keywords: periodic parametric instabilities, ion-plasma mode, high-intensity maintenance electric field, micro-discharges, microwave-excited discharges, electronic surface-wave mode

(Some figures may appear in colour only in the online journal)

1. Introduction

The intensity of the E-field actually driving the discharge, the maintenance E-field, cannot be varied simply by raising or decreasing the externally applied RF and microwave powers or the applied dc voltage; this fact has long been ignored. As an example, consider that some researchers still believe that sustaining a microwave discharge with a high-Q resonant cavity will provide higher field amplitude in the discharge than with another type of microwave-field applicator, hence yielding higher excited states of atoms and molecules. As a matter of fact, igniting the discharge should be easier with such a resonant cavity but, under steady-state conditions, the maintenance E-field intensity (for a given discharge tube and EM power frequency) would remain approximately the same since the E-field intensity under ambipolar diffusion conditions is set by the dimensions of the discharge vessel for a given gas and pressure [1, 2].

The analysis developed in the current paper results from experiments performed with a specific configuration of microwave-field applicator, with which periodic parametric instabilities were observed [3]. According to the parametric instability model elaborated by Aliev and Silin [4], the generation of a wave at the ion-plasma frequency rather than at lower frequencies of the ion-acoustic wave dispersion relation requires an intense E-field. Such a field is defined as corresponding to an x/λ_{De} ratio equal to or greater than unity, where x is the oscillation amplitude of electrons in the E-field (also called the electron excursion parameter) and λ_{De}, the electron Debye length.

1.1. Summary of the theoretical features of periodic parametric instabilities generated in the intense maintenance E-field of a microwave discharge

1.1.1. Physical basis of the generation of the ion-plasma wave in an intense electromagnetic (EM) field. The expression for the electron oscillation amplitude in the microwave field (excursion parameter) $x = eE_0/m\omega_0{}^2$ indicates that it depends linearly on the electric field amplitude E_0 (e is the unsigned charge on an electron, m its mass and ω_0 the microwave field angular frequency). Figure 1 suggests that for $x > \lambda_{De}$, ions are no longer hindered in their movement by the electrostatic field of electrons, thereby oscillating collectively at their natural frequency f_{pi}.

1.1.2. Dispersion relation for ion acoustic (sound) waves in a discharge under weak E-field. Provided that the ion temperature T_i is low compared to that of electrons T_e, the dispersion equation covering the whole spectrum of ion oscillations, namely the ion-acoustic wave dispersion, can be expressed as:

$$\omega_{LF}^2 = \omega_{pi}^2 \frac{k_{LF}^2 \lambda_{De}^2}{1 + k_{LF}^2 \lambda_{De}^2}, \tag{1}$$

where ω_{pi} is the angular frequency of ion-plasma oscillations, ω_{LF} the angular frequency of the ion-acoustic wave and k_{LF} its wavenumber ($k_{LF} = 2\pi/\lambda_{LF}$). It is interesting to consider the two extreme values of $k_{LF}\ \lambda_{De}$ with respect to unity in this relation:

(i) when $k_{LF}\ \lambda_{De} \ll 1$, expression (1) yields $\omega_{LF} = \omega_{pi}(k_{LF}\ \lambda_{De})$, where ω_{LF} therefore takes values much lower than ω_{pi}; as a matter of fact, in this limit one can write: $\omega_{LF} = (T_e/M_i)^{1/2} k_{LF}$, which corresponds to a sound wave propagating in plasma;

(ii) when $k_{LF}\ \lambda_{De} \gg 1$, ω_{LF} then tends towards ω_{pi}. However, as a rule it is difficult to excite such an oscillation in plasma.

1.1.3. Dispersion relation for ion acoustic (sound) waves in a discharge under intense E-field. Aliev and Silin's model [4] predicts, and they were the first to come to such a conclusion, that in an intense EM field ($x \geqslant \lambda_{De}$), the angular frequency ω_{LF} of the ion acoustic wave tends toward ω_{pi}, even though $k_{LF}\ \lambda_{De} \leqslant 1$, in contrast to the case of a weak E-field. They found that the dependence of ω_{LF} on x for a given λ_{De} is actually provided by the following expression:

$$\omega_{LF}^2 = \omega_{pi}^2 \left[1 - \frac{J_0^2(\mathbf{k}_{LF} \cdot \mathbf{x})}{1 + (k_{LF}\lambda_{De})^2} \right], \tag{2}$$

where J_0 is the Bessel function of the first kind and of order zero. This relation is plotted in figure 2 for different x/λ_{De} ratios. In the case of no applied E-field, or of a weak one ($x \approx 0.1\ \lambda_{De}$), the corresponding curve is that of the wave dispersion (1), i.e. that of the usual ion-acoustic wave. However, for $x = \lambda_{De}$, the ion-acoustic wave transforms into an ion wave over a large range of the $k_{LF}\ \lambda_{De}$ product as compared to that for $x \approx 0.1\ \lambda_{De}$. Their model, in addition, expects a slightly varying decrease (less than $\approx 5\%$) of f_{LF} with respect to f_{pi} as a function of $k_{LF}\ \lambda_{De}$, as can be seen in figure 2 for $x/\lambda_{De} = 4$ and 7.

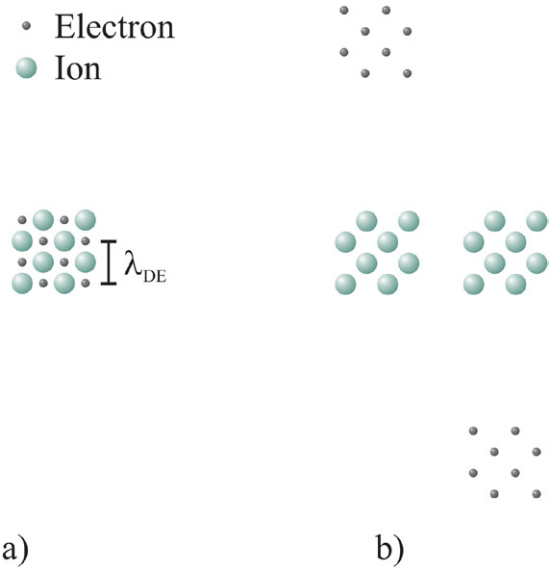

Figure 1. Idealized schematic representation in absence of collisions of the action of an EM field upon electrons; (a) whenever the amplitude of oscillation of the electrons x remains smaller than the electron Debye length λ_{De}; (b) when $x \approx 5\ \lambda_{De}$, the electrons being forced to move over a distance greater than λ_{De}; the ions can then travel freely and oscillate collectively at their natural frequency.

1.1.4. Landau damping of ion-acoustic waves and periodic instability growth rate. In a low-intensity EM-field and in the wavenumber range $k_{LF}\ \lambda_{De} \leqslant 2$, the ion-acoustic wave is heavily Landau damped, mainly as a result of its interaction with electrons [4]. However, the situation changes completely when a periodic E-field of high enough intensity is present, leading to the growth of a periodic parametric instability[4]; figure 3 shows that an ion wave is then generated even for $k_{LF}\ \lambda_{De} \leqslant 2$ (with frequency close to f_{pi}). As a matter of fact, the growth rate of periodic instability is significant only over a small $k_{LF}\ \lambda_{De}$ range, namely around $k_{LF}\ \lambda_{De} \approx 2$ for $x / \lambda_{De} = 1$ and around $k_{LF}\ \lambda_{De} \approx 0.5$ for $x / \lambda_{De} = 4$, as can be seen in figure 3. It means that its observation is expected to be limited to these low $k_{LF}\ \lambda_{De}$ values.

Recall that the generation of periodic parametric instability obeys the following selection of rules for frequency and wavenumber:

$$f_0 = f_{LF} + f_{pe} \quad \text{kinetic energy conservation}, \tag{3}$$

$$\mathbf{k}_0 = \mathbf{k}_{LF} + \mathbf{k}_{pe} \quad \text{momentum transfer conservation}. \tag{4}$$

Since we have just shown above that the wavelength of the ion mode parametrically generated is of the order of λ_{De}, which is very small compared to the wavelength of the pump field, it allows us to consider that the pump wavenumber $\mathbf{k}_0$ is comparatively close to zero, which means the electronic and ionic wave are excited in opposite directions. Therefore, in the present case, $|k_{pe}| = |k_{pi}| = k$ [5].

[4] This comes from the fact that the velocity of electrons in the EM field is then higher than the thermal velocity, which is responsible for Landau damping.

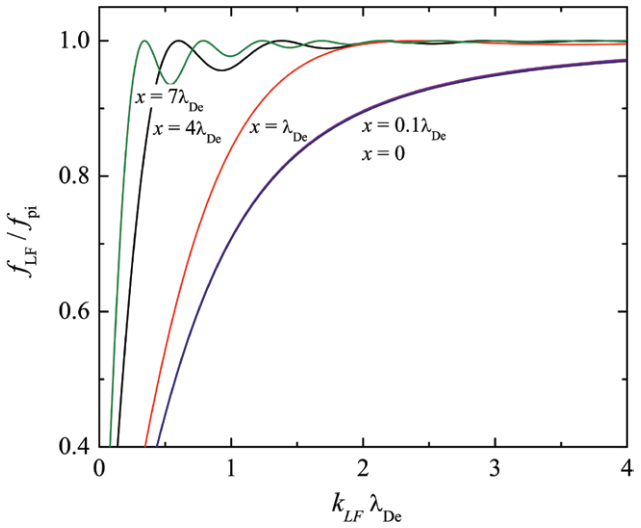

Figure 2. Calculated dispersion plot of the ion-acoustic wave according to relation (2) from [4] in a plasma subjected to an EM field, at different values of the x/λ_{De} ratio. The ion-acoustic wave observed at low E-field intensity ($x \leqslant 0.1\ \lambda_{De}$) transforms into an ion wave for $x \geqslant \lambda_{De}$, even though $k_{LF}\ \lambda_{De} < 1$.

A further comment is that the formalism of Aliev and Silin can be extended to various combinations of particle oscillation modes. For example, the electronic wave-mode could be excited either very close to f_{pe} (underdense plasma) or at the electron plasma frequency of a propagating surface wave (overdense plasma) so the $f_{SW} \approx f_{pe} / (1 + \varepsilon_r)^{1/2}$ where ε_r is the relative permittivity of the dielectric medium, possibly a lower density plasma, surrounding the (high density) plasma [3].

1.2. Summary of the experimental observations concerning the periodic parametric instabilities generated in the intense maintenance E-field provided by the specific microwave field-applicator described in the current paper

The detection of the signals generated by the E-field pump with the microwave field-applicator used (to be described further below) is achieved with a spectrum analyser, which enables us to record EM signals generated over a very broad spectral range (in our case ≈ 100 kHz–3 GHz) ([3] for details). Figure 4 is an example of a typical recording stemming from an applied EM-field pump at frequency $f_0 = 2.2$ GHz (microwave domain), sustaining an H_2 discharge. The first 'line' (side-band) on the left of the pump signal f_0, denoted f_{pe}, corresponds to the generation of an electronic wave. The frequency difference between f_0 and f_{pe} is equal to the ion-plasma mode generated at frequency f_{pi}: these three frequencies are related by selection rule (3). The first side-band on the right of the pump frequency, i.e. at $f_0 + f_{pi}$ is termed an anti-Stokes line, and it results from the non-linearity of the parametric instability process. It is worth noting that the various side-bands (lines) recorded are quite sharp spectrally speaking. According to Drake *et al* [6], this comes from the fact that $k_{LF}\ \lambda_{De} < 1$, and the lower this product, the sharper the recorded line is expected to be. In contrast, in many reported experiments (most probably at lower E-field intensity), ion oscillations are observed at lower frequencies than the ion-plasma frequency

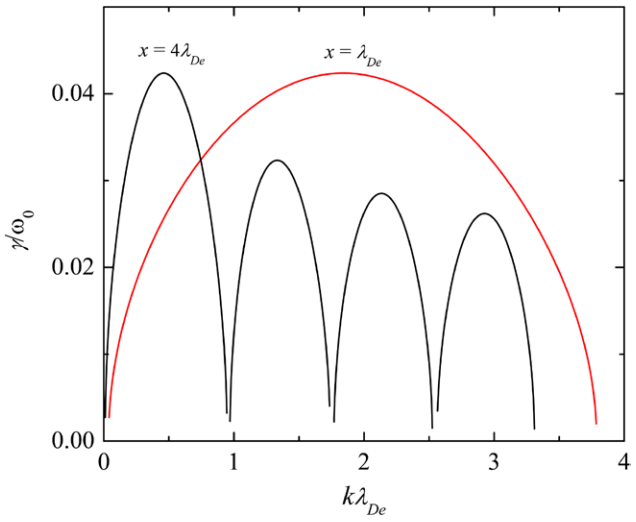

Figure 3. Calculated ratio of the periodic parametric instability growth rate γ over the pump angular frequency ω_0 as a function of $k\lambda_{De}$ ($T_e = 100\ T_i$ where T_e and T_i are the electron and ion temperatures, respectively) [4].

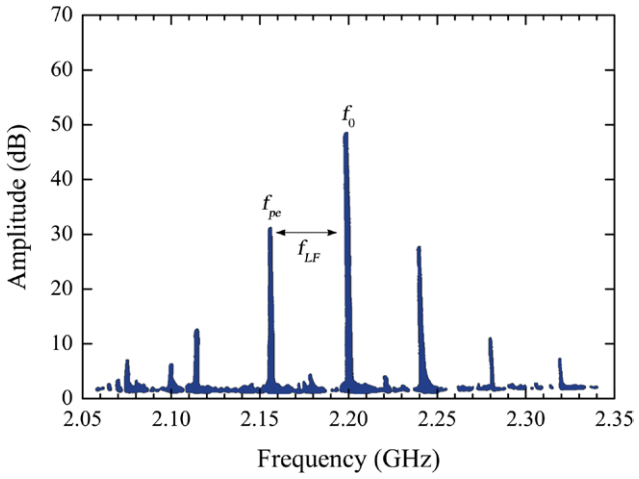

Figure 4. Amplitude (dB units) of the EM signal recorded on a spectrum analyser when sustaining an H_2 discharge (≈100 mtorr: 13 Pa), under intense maintenance E-field conditions, with an applied microwave field at a frequency of f_0. Side-bands are generated on both sides of the pump-field frequency f_0, which correspond to the excitation of an electron-plasma wave at a frequency of f_{pe} or its harmonics. The frequency difference between f_0 and f_{pe}, denoted f_{LF}, corresponds to the simultaneous excitation of an ion-plasma mode, in agreement with selection rules (3). The recorded emission is of the Sv type [3].

and, furthermore, are spectrally large and noisy (e.g. Aihara *et al* [7]).

Additional theoretical and experimental details on parametric instabilities can be found in existing, but not very recent, literature. Porkolab and Chang [5] have dedicated part of their exhaustive paper on non-linear wave effects in plasmas to experiments related to parametrically induced oscillations. It turns out that a lot of attention has been paid by various authors to the theoretical derivation of threshold expressions for the occurrence of parametric instabilities in homogeneous and inhomogeneous plasmas, for instance, as well as for determining experimentally how much power (generally not translated into power density) is needed to observe them. As far as we know, the current work is the first one to connect the manifestation of ion-plasma oscillations due to parametric instabilities not close to threshold conditions, but far above them, namely under $x/\lambda_{De} \geqslant 1$ conditions, and to develop the physical principles enabling one to obtain discharges with such a large x/λ_{De} ratio.

2. Power balance relating the power lost per electron through collisions with heavy particles to the power absorbed per electron over a period of the EM field

We need to dwell on the power balance equation on which our calculations leading to the value of the x/λ_{De} ratio are based. This section is divided into two parts: the local power balance relation such as that found in a surface-wave discharge, for example, and a more general case where power balance is not local but global[5]. The latter requires us to consider separately two distinct volumes: the volume over which microwave power is absorbed (by electrons) and the volume over which electrons lose their power through collisions with heavy particles, as is the case in the specific microwave discharge described in the current paper.

2.1. The case where the power absorbed per electron (over a period of the EM wave), θ_A, is locally related to the power lost per electron through collisions with heavy particles, θ_L

In what follows, the plasma column sustained by an EM surface wave is analysed as a mere example of the local power balance case. As illustrated in figure 5, the power extracted between axial positions, z and $z + dz$ from the power flow $P(z)$ of the surface wave propagating along the plasma column, is absorbed (to sustain the discharge) within the infinitesimally small cylindrical gas-slab also confined between z and $z + dz$. The power transfer from the wave to the discharge is thus achieved axial segment by axial segment, one after the other towards the end of the plasma column, and in that sense can be termed local.

The mathematical expressions (5)–(7) display the quantities involved in the power transfer from the wave flow to the discharge of gas. First of all, relation (5) provides the value $P(z)$ of the wave power flow available at z (power distributed over a plane perpendicular to the tube axis and extending from $r = R$ (plasma column radius) up to $r = \infty$ where r is the radial position from the axis of the plasma column) as a function of the wave attenuation coefficient $\alpha(z)$ at this axial position:

$$P(z) = P(0)\exp\left\{-2\int_0^z \alpha[\bar{n}(z)]\mathrm{d}z\right\}, \qquad (5)$$

[5] The expression 'local power balance' in our specific context means that both the absorbed microwave power and the power lost by collisions from electrons with heavy particles are dissipated within the same volume whereas the 'global power balance' refers to the situation where microwave power is absorbed in a smaller volume than the diffusion volume in which this power is dissipated.

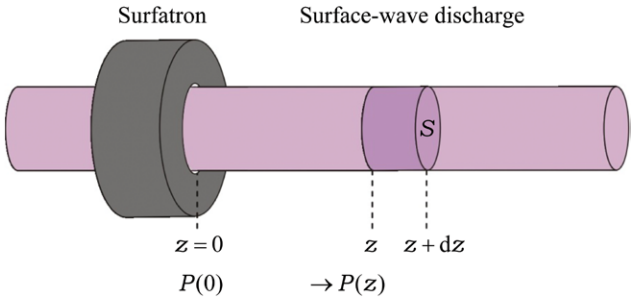

Figure 5. Schematic representation of the power transfer from a propagating surface wave to the discharge column that it sustains; the power extracted from the wave flow $P(z)$ between z and $z + \mathrm{d}z$ is absorbed into the discharge tube within the same axial segment delimited by z and $z + \mathrm{d}z$, and is assumed to be dissipated within this same axial segment.

where the axial value of the attenuation coefficient depends on $\bar{n}(z)$, the electron density averaged over the cross-section S of the plasma column at this axial position. Relation (6) indicates how to determine, under these conditions, $-\mathrm{d}P(z)$, the amount of power extracted from the wave between z and $z + \mathrm{d}z$. Equation (7) connects the power taken from the wave flow (left-hand side term) to the power absorbed in the discharge within the corresponding z, $z + \mathrm{d}z$ slab, introducing for that purpose the parameter $\bar{\theta}_\mathrm{A}$, which is the power absorbed per electron over a wave period as averaged over the plasma column cross-section S [8]:

$$-\mathrm{d}P(z) = 2\alpha[\bar{n}(z)]P(z)\mathrm{d}z, \tag{6}$$

$$2\alpha[\bar{n}(z)]P(z) = \bar{\theta}_\mathrm{A}(\bar{n})\bar{n}\,S. \tag{7}$$

In a plasma sustained by an EM field of angular frequency ω_0 and, in the present case, with a relatively weak electron-neutral collision frequency ν for momentum transfer ($\nu^2 \ll \omega_0^2$), the expression for θ_A is given by [1, 2]:

$$\theta_\mathrm{A} = \frac{e^2\nu {E_0}^2}{2m{\omega_0}^2}, \tag{8}$$

where E_0 is the amplitude of the maintenance E-field driving the discharge. Under a steady-state regime, considering local power transfer as defined, the absorbed power θ_A per electron adjusts itself to compensate exactly for θ_L, the power lost per electron due to their collisions with heavy particles, and we thus have:

$$\theta_\mathrm{A}(E) = \theta_\mathrm{L}(<U_\mathrm{eV}>), \tag{9}$$

where $<U_\mathrm{eV}>$ is the average electron energy. As a matter of fact, if the power θ_A was smaller than θ_L, the discharge would go off; on the other hand, if θ_A was larger than θ_L, the electron density of the plasma would increase, contradicting both cases with our assumption of a steady-state discharge. Relation (9) therefore constitutes the balance equation between the power gained and the power lost per electron in the plasma[6], whenever the power transfer is local. Equation (9) also means, and this consequence must be emphasized, that the intensity of E_0, the amplitude of the maintenance E-field (related to θ_A by (8)) adapts itself to compensate exactly for the power lost θ_L.

In the specific case where the charged particles are lost by diffusion to the tube wall on which they recombine, any increase in these losses leads to an increase in the electron average energy [1, 2], i.e. in the value of T_e in the case of a Maxwellian electron energy distribution function (EEDF). As a result, the value of $\theta_\mathrm{L}(<U_\mathrm{eV}>)$ increases when the losses of charged particles increase. Recall that under ambipolar diffusion regime, in principle T_e depends only on the discharge vessel configuration and dimensions and on the nature of the gas and its pressure, which we designate as the operating conditions, possibly including the operating frequency but excluding the applied RF and microwave power or dc voltage. Therefore, the intensity of the discharge maintenance E-field, appearing in θ_A (8) is set by θ_L through relation (9), i.e. as already mentioned, it depends only on the operating conditions. Said differently, θ_L is the dominant quantity in the power balance (9) as θ_A adjusts to it. In the case of the positive column of a dc discharge, the maintenance E-field is not determined by the applied voltage across the discharge tube, but by the particle losses, the difference between the externally applied voltage and that across the positive column showing up as the sum of voltages across the various luminous and dark zones of the discharge.

2.2. The case where power balance is not achieved locally because the volume over which the E-field power is absorbed by the electrons is smaller than the diffusion volume over which they lose the power acquired (high intensity E-field conditions)

Such a non-local power balance can be analysed, in an innovative way, by resorting again to the parameters θ_A and θ_L. In the current paper, we consider the case where the absorption volume, V_1, is smaller than the diffusion (expanding plasma) volume, V_2. The global balance, again neglecting Joule and sheath losses for simplicity at this point, imposes that:

$$\theta_\mathrm{A} n_{\mathrm{e}1} V_1 = \theta_\mathrm{L} n_{\mathrm{e}2} V_2 \tag{10}$$

where $n_{\mathrm{e}1}$ and $n_{\mathrm{e}2}$ are the electron density in the absorption and diffusion volumes, respectively. This imposes in the end that:

$$\theta_\mathrm{A}/\theta_\mathrm{L} > n_{\mathrm{e}2}/n_{\mathrm{e}1}. \tag{11}$$

The results of the numerical calculations presented in section 3, which include Joule and sheath losses not considered in (10) and (11), will confirm that $n_{\mathrm{e}2}/n_{\mathrm{e}1}$ is smaller than unity. Therefore, the value of θ_A is actually greater than that of θ_L. This contrasts with the case of local power balance, where they are (approximately) equal, and inequality (11) implies, through relation (8), that the intensity of the maintenance E-field is in fact greater. Such conditions lead to a generic method allowing an increase in the intensity of the maintenance E-field. As we will show, these conditions are best obtained with non-homogeneous plasmas, as is the case with

[6] The above considerations neglect, for the sake of presentation, the power lost (Joule heating) in the dc ambipolar electric field as well as that lost in the plasma sheath. These contributions, which are taken into account further on in our model, are also local and therefore do not affect the basis of our reasoning.

the specific microwave discharge to be described in the next section.

3. Description of a microwave discharge system providing a high intensity maintenance *E*-field allowing observing periodic parametric instabilities

3.1. Experimental arrangement and settings

Figure 6 is a schematic drawing of the microwave field-applicator ensuring a discharge with a maintenance *E*-field of high enough intensity so that periodic parametric instabilities can be excited. Two antennas are used to sustain the discharge with microwave power, which are positioned diametrically opposed along a tube diameter line, defining the z-axis. These are each made from a straight segment of a 50 Ω semi-rigid coaxial cable ($\approx$2.2 mm outside diameter), the inner conductor of which, on the radiative side, protrudes from the outer conductor by a few mm before being soldered to a cylindrically flat conductor (2 mm diameter), thereby defining the microwave radiating surface. These antennas lean against the outer wall of the discharge tube, which is made from fused silica, a dielectric material transparent to microwave radiation.

The power supplied by the microwave generator is separated into two equal parts (with a 3 dB power divider) and a 180° phase difference between these two antennas is achieved with a phase shifter ($\Delta\varphi$) tuned for minimum intensity of the f_0 pump signal detected, on a spectrum analyser, from an antenna located at 90° from the z-axis. Such a setting ensures that the resulting *E*-field emanating from the antennas is mainly directed along the z-axis, mostly confined within a virtual cylinder—defined by the diameter of the radiative end-plates of the two antennas—and extending all along the discharge tube diameter. These antennas are held in place by a cylindrical metallic (brass) structure closed at both ends to avoid radiation in the room. This assembly also forms a resonant cavity as a means of determining, whenever needed, the electron density in the discharge through measurement of the frequency shift on its TM_{010} mode.

Figure 7 is an artist's view of the actual microwave field-applicator (a) schematizing the cylindrical absorption volume (red) and the diffusion volume (pink), and (b) and (c) indicating the direction of the *E*-field lines in two perpendicular cut planes.

3.2. Simplified representation of the microwave field-applicator assumed in the numerical model

To reduce computing time, the above discharge system has been reduced to a 2D configuration. The vertical axis along which the coaxial cables supporting the antennas are aligned becomes a symmetry axis (z-axis), imposing a two-dimensional (2D) axisymmetric configuration. Figure 8(a) displays a general view of this 2D simplified configuration while figures 8(b) and (c) show the (approximate) direction of the microwave *E*-field lines in two perpendicular cut planes.

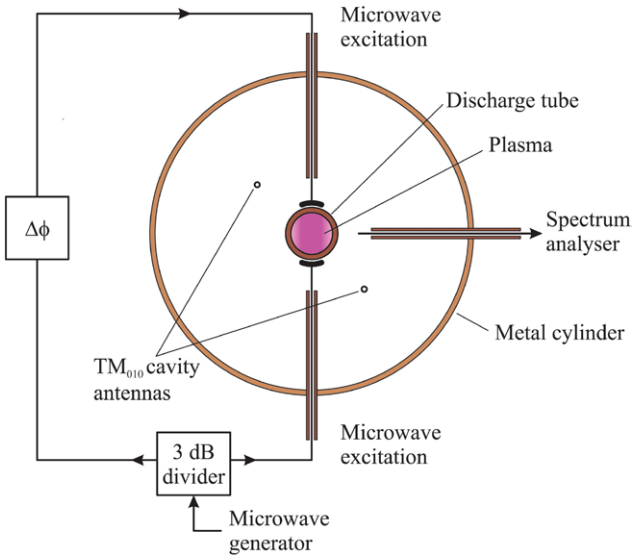

Figure 6. Schematic cross-sectional view of the microwave-field applicator utilized for achieving a high intensity maintenance field in the discharge. Two antennas are used to sustain the discharge with microwave power (see text). The power coming from the generator goes through a 3 dB power divider, which provides an equal amount of power on each antenna. A 180° phase difference between the field radiated by these two antennas is achieved with a phase shifter ($\Delta\phi$) tuned for minimum intensity of the f_0 (pump) signal detected at 90° on the spectrum analyser. These antennas are held in place by a cylindrical metallic (brass) structure, closed at both ends to avoid radiation in the room. This assembly also serves, whenever needed, as a means of determining the electron density in the discharge through measurement of the frequency shift on the TM_{010} mode of this cavity.

4. Hydrodynamical model of the microwave discharge system

4.1. Governing equations

A numerical simulation of the current microwave discharge has been performed using COMSOL© Multiphysics software with RF (including microwaves) and Plasma Modules (version 4.1). This software is a powerful, finite element, partial differential equation solution-engine. The discharge is described as a hydrodynamic fluid based on features of the plasma model reported in the COMSOL Plasma Module User's Guide [9], which refers to the handbook of Lieberman and Lichtenberg [10].

The plasma is assumed to be composed of electrons and heavy species (atoms in ground state or in excited—metastable—states, and their ions) forming a dilute gas. The heavy species temperature (gas temperature) is assumed to be uniform in space and is the same for all species. The mass averaged gas velocity is equal to zero.

The model consists of a set of equations for the high frequency electric field and the electrostatic (dc) ambipolar field, the densities of electrons and heavy species, and the electron energy. Elements of this model can also be found in Lee *et al* [11] and Gregório *et al* [12] for instance.

4.1.1. High frequency and dc (ambipolar) field equations. The high frequency (HF) periodic electric field present in the discharge, $\mathbf{E}_{HF}$, is governed by the equation following

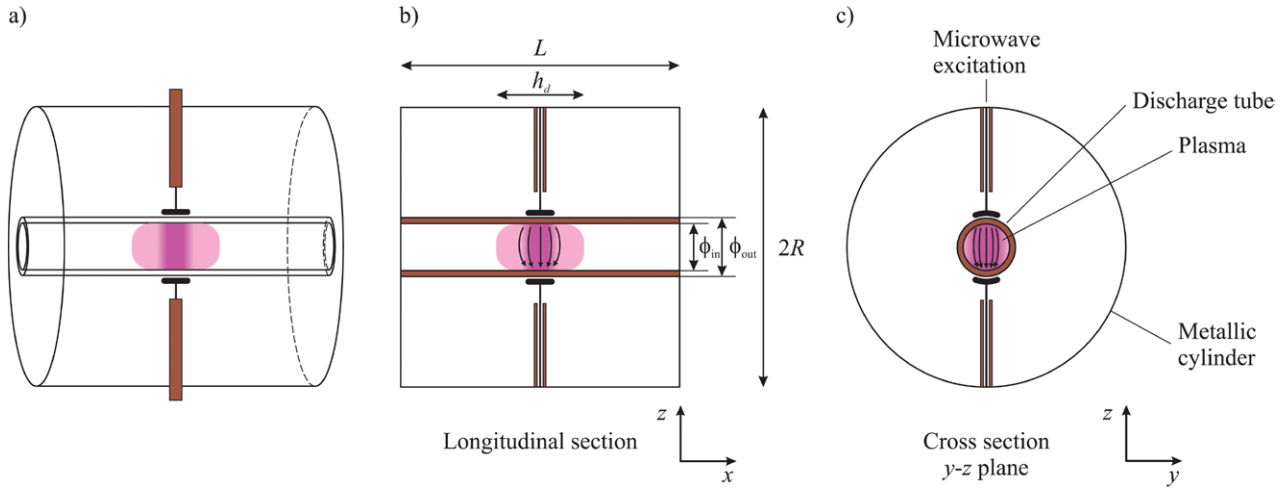

Figure 7. Schematized representation of the actual microwave field applicator with an artist's view (a) of the microwave power absorption zone (violet) and diffusion zone (pink), and of the approximate direction of the *E*-field lines generating the discharge in two perpendicular cut planes (b) and (c).

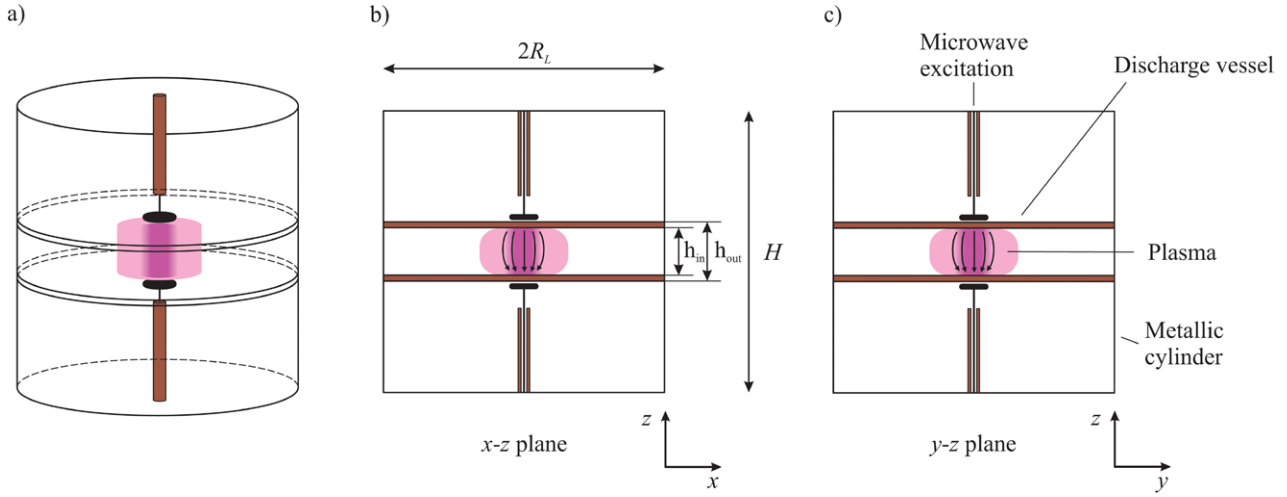

Figure 8. Simplified 2D axisymmetric configuration of the field-applicator where *z* is the axis of symmetry: (a) general view of the configuration displaying the microwave power absorption zone (red) and diffusion zone (pink), and (b) and (c) showing accordingly the direction of the *E*-field lines in two perpendicular cut planes.

from the combination of the two Maxwell equations bearing the rotational operator:

$$\nabla \times (\nabla \times \mathbf{E}_{\mathrm{HF}}) - {k_0}^2 \varepsilon_{\mathrm{r}} \mathbf{E}_{\mathrm{HF}} = 0, \tag{12}$$

where ε_{r} is the relative (to vacuum) complex electric permittivity of the medium, $k_0 = \omega/c$ is the free-space wavenumber, ω_0 is the HF electric field angular frequency, c is the velocity of light in a vacuum and $\sqrt{\mathbf{E}_{\mathrm{HF}}\mathbf{E}^*_{\mathrm{HF}}} = E_0$ is the amplitude of the maintenance electric field. When plasma is the medium of interest, its relative complex electric permittivity ε_{r} is calculated from the Lorentz cold-plasma formula:

$$\varepsilon_{\mathrm{r}} = 1 - \frac{\omega_{\mathrm{pe}}^2}{\omega_0\,(\omega_0 - j\nu)}, \tag{13}$$

where $\omega_{\mathrm{pe}} = n_{\mathrm{e}} e^2/(\varepsilon_0\, m)$ is the electron-plasma angular frequency, n_{e} is the electron number density and ε_0 the free-space permittivity.

The electron density, n_{e}, and electron energy density, n_ε, are calculated from the following set of drift-diffusion equations:

$$\frac{\partial}{\partial t}(n_{\mathrm{e}}) + \nabla \cdot \mathbf{\Gamma}_{\mathrm{e}} = R_{\mathrm{e}}, \tag{14}$$

$$\frac{\partial}{\partial t}(n_\varepsilon) + \nabla \cdot \mathbf{\Gamma}_\varepsilon + \mathbf{E}_{\mathrm{a}} \cdot \mathbf{\Gamma}_{\mathrm{e}} = S_\varepsilon + Q_{\mathrm{rh}}, \tag{15}$$

where R_{e} is the net creation rate of electrons, Q_{rh} is the density of power absorbed by the electrons from the electromagnetic *E*-field and S_ε is the net loss of electron power per unit volume due to electron-neutral collisions in the bulk-plasma volume, and $\mathbf{E}_{\mathrm{a}} \cdot \mathbf{\Gamma}_{\mathrm{e}}$ is the Joule heating resulting from the electrostatic (dc) ambipolar field $\mathbf{E}_{\mathrm{a}}$. The vectors $\mathbf{\Gamma}_{\mathrm{e}}$ and $\mathbf{\Gamma}_\varepsilon$ represent the total (drift and diffusion) flux of electrons and that of electron energy, respectively. These are given by:

$$\mathbf{\Gamma}_{\mathrm{e}} = -n_{\mathrm{e}}(\mu_{\mathrm{e}} \mathbf{E}_{\mathrm{a}}) - D_{\mathrm{e}} \nabla n_{\mathrm{e}} \tag{16}$$

and

$$\mathbf{\Gamma}_\varepsilon = -n_\varepsilon(\mu_\varepsilon \mathbf{E}_a) - D_\varepsilon \nabla n_\varepsilon, \tag{17}$$

where μ_e is the electron mobility, D_e is the electron diffusion coefficient, μ_ε is the energy mobility and D_ε is the electron energy diffusivity.

4.1.2. Bulk plasma expressions. The quantities R_e and S_ε appearing in equations (14) and (15) respectively are determined by the plasma chemistry (section 4.2) and are calculated correspondingly from:

$$R_e = \sum_{j=1}^{M} x_j k_j N_n n_e, \tag{18}$$

$$S_\varepsilon = \sum_{j=1}^{P} x_j k_j N_n n_e \Delta\varepsilon_j - \frac{3}{2}\delta n_e \nu k_B (T_e - T), \tag{19}$$

where x_j is the mole fraction of the target species for reaction j, k_j is the rate coefficient to achieve reaction j, N_n is the total number density of the neutral species and $\Delta\varepsilon_j$ is the energy loss following reaction j. Summation (18) runs over the number M of reactions that contribute to the growth or decay of electron density. Summation (19) runs over the total number P of the various types of inelastic electron-neutral collisions, T is the gas temperature, T_e is obtained from $T_e = (2/3)\bar{\varepsilon}$ with $\bar{\varepsilon}$ being the mean electron energy defined as $\bar{\varepsilon} = n_\varepsilon/n_e$, δ is the fraction of energy lost in an electron-heavy species elastic collision, and k_B is the Boltzmann constant.

The rate coefficients are computed from the corresponding cross-section data using the well-known integral:

$$k_j = \gamma \int_0^\infty \varepsilon \sigma_{cj}(\varepsilon) f(\varepsilon) \mathrm{d}\varepsilon \tag{20}$$

where $\gamma = (2e/m)^{1/2}$, ε is the electron energy, σ_{cj} is the collision cross-section for electrons to achieve reaction j, and $f(\varepsilon)$ is the electron energy distribution function.

4.1.3. Mass transport equations. The number density n_k of each heavy species k can be derived from the mass transport equations, which have the form:

$$\rho \frac{\partial w_k}{\partial t} + \nabla \cdot \mathbf{j}_k = \mathbf{R}_k \tag{21}$$

where ρ denotes the mass density of the gas mixture, w_k designates the mass fraction of the kth species, $\mathbf{j}_k$ is the diffusive flux vector, and R_k is the rate expression for species k, with $k = 1\ldots(Q-1)$, where Q is the number of the various heavy species. In our model, $Q = 3$, the heavy species are Ar, Ar^+ and Ar_m. The mass fraction for $k = Q$, which is that of the uncharged species Ar, is obtained from the sum of the mass fractions of all species since it must be equal to unity:

$$w_Q = 1 - \sum_{k=1}^{Q-1} w_k \tag{22}$$

Then, n_k is provided by:

$$n_k = \rho\, w_k. \tag{23}$$

The diffusive flux vector of the kth species is expressed as:

$$\mathbf{j}_k = \rho w_k \mathbf{V}_k \tag{24}$$

where $\mathbf{V}_k$ is the diffusion velocity for species k. It can be found from:

$$\mathbf{V}_k = -D_k \frac{\nabla w_k}{w_k} - \frac{D_k^T}{\rho w_k}\frac{\nabla T}{T} + Z_k \mu_k \mathbf{E}_a, \tag{25}$$

where D_k is the corresponding diffusion coefficient and D_k^T the thermal diffusion coefficient for species k, Z_k is the charge number for species k, and μ_k is the mobility for species k. The first term on the RHS of (25) yields the velocity connected with the kth species non-uniformity, the second term has to do with temperature non-uniformity and the third term represents the species migration in the electrostatic field. It is assumed in the current model that all heavy particles have the same temperature, which is equal to the gas temperature. Since gas temperature is assumed uniform, the second term on the RHS drops. The third term is additionally zero for neutral particles.

The density of the gas is given by the ideal gas law as:

$$\rho = \frac{pM_m}{RT}, \tag{26}$$

where p is the gas pressure, M_m is the mean molar mass of the heavy species mixture, and R is the universal gas constant.

The rate expression for species k, R_k, used in (21) is determined by the stoichiometry of the system through the formula:

$$R_k = M_k \sum_{j=1}^{N} v_{kj} r_j, \tag{27}$$

where M_k is the molar mass of species k, v_{kj} is the stoichiometric matrix and r_j is the reaction rate corresponding to reaction j and the index j runs over the number N of reactions in which species k is involved.

The potential of the electrostatic field, V, which is connected to the ambipolar field by the relation $\mathbf{E}_a = -\nabla V$, is computed using Poisson's equation:

$$-\nabla \cdot \varepsilon_0 \nabla V = \rho_V, \tag{28}$$

where the space charge density, ρ_V, is calculated from the formula:

$$\rho_V = e\left(\sum_{k=1}^{N} Z_k n_k - n_e\right). \tag{29}$$

Note that the quasi-neutrality of the plasma and the existence of ambipolar diffusion are not assumed *a priori* in the model, in which the diffusion of electrons and ions is described by equations comprising the diffusion coefficients specific to each species. However, in the end, the conditions for the quasi-neutrality of the plasma and ambipolar diffusion within it are found to be fulfilled, and they are the result of the initial assumptions of the model.

4.2. Plasma chemistry

Plasma chemistry refers to the gas phase being 'heated' until some electrons are no longer associated with their parent

Table 1. Plasma particles involved in the collisions considered and the nature of their corresponding reactions accounted for in the model.

Reaction	Formula	Type	$\Delta\varepsilon$ (eV)
1	$e + Ar \rightarrow e + Ar$	Elastic	0
2	$e + Ar \rightarrow e + Ar_m$	Excitation	11.5
3	$e + Ar_m \rightarrow e + Ar$	Superelastic	−11.5
4	$Ar_m + Ar \rightarrow Ar + Ar$	Metastable quenching	—
5	$e + Ar \rightarrow 2e + Ar^+$	Ionization from a ground-state atom	15.8
6	$e + Ar_m \rightarrow 2e + Ar^+$	Ionization from a metastable-state atom	4.24
7	$Ar_m + Ar_m \rightarrow e + Ar + Ar^+$	Penning ionization	—

Table 2. Surface quenching of metastable-state atoms and surface recombination of ions accounted for in the model with their sticking coefficient (probability).

Reaction	Formula	Sticking coefficient
1	$Ar_m \rightarrow Ar$	1
2	$Ar^+ \rightarrow Ar$	1

atom. Four plasma species are involved in the current case, namely electrons, neutral argon atoms, metastable-state argon atoms and positive argon ions designated as e, Ar, Ar_m, Ar^+, respectively. Their mutual (binary) interactions are accounted for in the model by the seven reactions displayed in table 1.

Reaction 1 describes the elastic process whereby electrons collide with argon atoms in their ground state, these atoms remaining in such a state after collision. Excited argon atoms are produced through collisions with electrons while their de-excitation (reverse process) is possible via superelastic collisions with electrons. These two processes are expressed by reactions 2 and 3, respectively. As for metastable-state argon atoms, they can be de-excited (quenched) down to the ground state by another argon atom in its ground state (reaction 4). Electrons can be released from argon atoms as a result of ionizing reactions 5, 6 and 7; noteworthy is the stepwise ionization process where a metastable-state acts as an intermediate (relay) energy level (reaction 6), which allows low-pressure argon discharges to be sustained. Ionization can also be obtained by a Penning reaction following the interaction of two metastable-state argon atoms (reaction 7)[7]. Finally, electrons are lost as they recombine on the discharge tube wall after reaching it through diffusion. Equation (21) together with (27) and (23) are used to find Ar_m and Ar^+ number densities, while that of Ar is obtained from (22) and (23).

In addition to the preceding plasma-volume reactions, we consider the surface reactions of metastable-state atoms and argon ions, as depicted in table 2. When these species hit a surface, they are quenched and neutralized, respectively.

4.3. Species parameters

Solving equations (14) and (15) requires computing the quantities defined in expressions (16)–(20) in which the value of the species parameters D_e, D_ε, μ_e and μ_ε as well as k_j are needed. In the current model, k_j and μ_e are found using the BOLSIG$^+$ code, which allows us to numerically solve the two-term[8] Boltzmann equation for electrons in weakly ionized gases, possibly subjected to an uniform electric field. The 2014 solver version is described in a paper by Hagelaar and Pitchford [15], together with cross-sections for electron collisions taken from the Phelps database [16]. The parameters are calculated assuming that the rate of electron–electron (e–e) collisions is that determined by an electron number density equal to the critical electron density n_c. In such a case, owing to the low (neutral) gas pressure, the e–e collisions lead to Maxwellisation of the electron energy distribution function. As for the other electron coefficients, namely those of electron diffusion, energy diffusivity and energy mobility, these are calculated respectively from:

$$D_e = \mu_e T_e,\ D_\varepsilon = \mu_\varepsilon T_e,\ \mu_\varepsilon = \frac{5}{3}\mu_e. \tag{30}$$

Instead of calling on the macroscopic expressions (30), it is possible to compute these coefficients directly from the Boltzmann equation. We have performed calculations for both cases. The detailed results are slightly different, but the conclusions are the same.

The heavy species diffusion coefficients used in (21) are taken following [17]. The ion mobility μ_k is calculated using the Einstein relation:

$$\mu_k = \frac{eD_k}{k_B T}. \tag{31}$$

4.4. Limiting the extension of the calculation domain and boundary conditions

Due to the assumed symmetry of the system configuration (figure 8), the calculations only need to be performed on part of it. The restricted calculation domain with respect to the full system is shown in figure 9(a). The various corresponding parts of the system are identified by reference marks as indicated in figure 9(b).

The area of the ABCP rectangle figures that part of the discharge tube region considered in the calculations continuing freely beyond BC since it extends outside the cavity, while CP corresponds to the inner dielectric wall of the discharge tube. The rectangle CDOP delineates the corresponding inner and outer

[7] Considering that the possibility of ionizing through reactions 6 and 7 is essential in the present calculations as they lower the value of θ_A when compared to accounting only for direct ionization on the atom ground-state (reaction (5)): see section 4.2.4 in [1] and [14].

[8] The electron energy distribution function is expanded in terms of Legendre polynomials of cos θ (spherical harmonics expansion). In many cases, a two-term approximation already gives useful results [15].

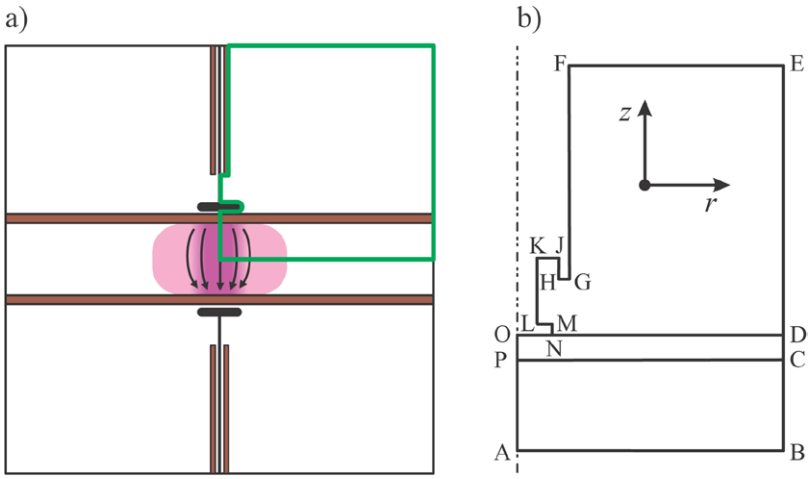

Figure 9. (a) Delimitation of the restricted calculation domain with respect to the whole system (figures 8(b) and (c)); (b) reference marks on the actual calculation domain. Point A is the coordinate centre. That part of the drawing corresponding to the microwave field applicator is not to scale.

Table 3. Identification of the boundaries encountered in the calculations as posted in figure 9(b), their nature and characteristic lengths.

Boundary designation	Description and nature	Length (mm)
AB	Symmetry plane along the discharge tube	10
BC	Open ended: inner part of the discharge tube as it extends outside the cavity	4
CD	Discharge tube inner and outer diameter dielectric walls (8/10 mm): fused silica	1
DE	Conductor	10
EF	Conductor	8.9
FG	Outer conductor of the coaxial cable	8.25
GH	Outer conductor thickness	0.26
HJ	Inner wall of the cable outer conductor	0.75
JK	Thickness of the coaxial cable dielectric core	0.789
KL	Bare length of the coaxial cable inner conductor	2.8
LM	Mounting plate (conductor) of the antenna (wave excitation) soldered to the coaxial cable inner conductor	0.949
MN	Thickness of the antenna mounting plate (conductor)	0.2
NO	Radiative surface of the antenna (conductor)	1
OP	Symmetry axis	1
PA	Symmetry axis	4
CP	Discharge tube inner wall (dielectric material: fused silica)	4
DO	Discharge tube outer wall (dielectric material: fused silica)	4

walls of the dielectric discharge tube, made from fused silica. Table 3 identifies the various boundaries encountered in the calculations, specifying their nature and providing their characteristic lengths. The coaxial cable supplying the microwave power, of the semi-rigid type, has a 50 Ω impedance. The diameter of its inner conductor is 0.51 mm, the diameter of the Teflon dielectric core (inner diameter of the outer conductor) is 1.68 mm and the outer diameter of the outer conductor is 2.20 mm.

Equation (12) for the microwave E-field is solved in the whole calculation region. Perfect conductor conditions are imposed on conducting surfaces. Boundary JK, where the microwave field flows out from the coaxial cable, is set as a coaxial-type port with the electric field intensity adjusted to obtain a given input microwave power. As for the electrostatic field, we assumed that its potential was continuous in the whole calculation domain and considered all metallic surfaces as grounded, i.e. $V = 0$ on them.

The equations for plasma species, namely (14), (15) and (21), and Poisson's equation (28) are solved only in the ABCP region. Symmetry conditions are imposed on AP and AB boundaries for all these equations. Boundary CP is treated as a surface on which the reactions listed in table 2 take place. As far as boundary conditions for electrons are concerned, we directly used COMSOL Wall Boundary Conditions (WBCs), assuming that reflection, thermal emission and secondary emission of electrons do not occur at the boundary. The fluxes of electrons and electron energy are then expressed respectively as $\mathbf{n} \cdot \Gamma_e = (1/2) v_{th} n_e$ and $\mathbf{n} \cdot \Gamma_\varepsilon = (5/6) v_{th} n_\varepsilon$, where v_{th} is the electron thermal velocity and $\mathbf{n}$ the outward normal vector. For details see the COMSOL User's Guide [9].

4.5. Validity of the calculation method and assumptions

As far as boundary conditions are concerned, comparison of the validity of the COMSOL WBCs with the more specific ones used by Hagelaar [15] can be found in the work of Rafatov [18], who shows that the difference between

the two sets of results lies within approximately 2%. The explanation for such a slight difference only can be found in Paunska *et al* [19] in their fluid modeling of an argon RF discharge. Applying comparatively dielectric and conducting boundary conditions to the discharge tube wall, these authors conclude that changes in the discharge structure occur essentially within the plasma sheath, therefore leaving the values of the plasma parameters in the discharge bulk almost unaffected.

Checks were achieved confirming that the calculations made in the specific domain displayed in figure 9 gave the same results as those obtained when considering the full domain (with accordingly modified boundary conditions). As expected, these extended calculations are more time-consuming. Furthermore, several mesh sizes were tested to ensure that the final solution does not depend on the their dimensions. The mesh used is a triangular unstructured one consisting of about 25×10^3 domain elements refined to size 0.02 mm in areas where large gradients of electric field could be expected. The maximum mesh element size is found in the no-plasma region where it is 1.5 mm.

Two main sources of inaccuracy can be expected in the present calculations: i) the first one comes from the assumption of a 2D axisymmetric configuration. Whereas the absolute values of the plasma parameters and electromagnetic field intensity are probably affected, it is believed that their qualitative behaviour as a function of increasing power density, from which our conclusions are drawn, remains the same; ii) the second one relates to the condition for ensuring diffusion conditions with respect to free-fall, which imposes a priori that the electron mean free-path be smaller than the smaller dimension of the discharge tube (provided the plasma is homogeneous, which it is not). In the present case, at a pressure of 100 mTorr (13 Pa) in argon and assuming an electron temperature of 4 eV, we get a calculated mean free path of 12 mm as compared to a discharge tube diameter of 8 mm, implying that our plasma is not totally under diffusion conditions. Nonetheless, this does not seem to prevent authors [20] to use diffusion equation in their numerical fluid model at even lower pressures (1 Pa in argon) to model the behaviour of a discharge sustained under electron cyclotron resonance (ECR).

5. Calculation results from the model and discussion

Our calculations have been performed for a discharge in argon gas sustained with the microwave system described in section 2.1 at a pressure of 0.1 Torr (13.3 Pa) and an applied field frequency of 2.45 GHz, assuming an axis-symmetric based 2D-description for the microwave discharge system. These calculations provide the spatial distribution of the plasma parameters as well as of the electromagnetic field intensity. Although, as already mentioned, the calculation domain is restricted to 1/4 of the system configuration (figure 9), presentation of the results is made more attractive by mapping them on half of the system configuration, as illustrated in figure 10.

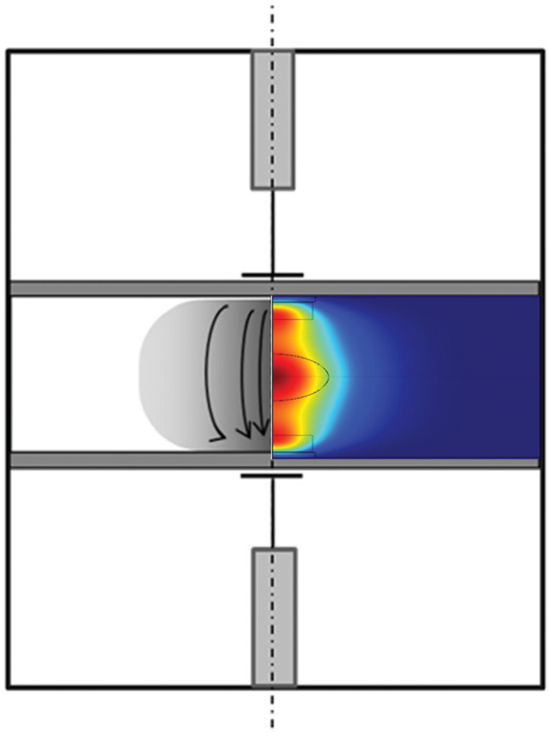

Figure 10. Coloured sketch showing the portion of the microwave-field applicator configuration over which the calculation results are to be displayed. Recall that the z-axis is directed along the dash–dot line while the y-axis extends perpendicularly from it towards the right side in the figure. The geometrical centre of the drawing in the figure corresponds to $z = 0$ and $y = 0$.

5.1. Mapping of the discharge plasma density

The electron density n_e, which increases with increasing absorbed microwave power, is always observed to reach its maximum value at $y = 0$, $z = 0$, as shown in figure 11. For an increasing absorbed power up to 2.4 W, n_e approaches the critical electron density n_c, which is defined by $\omega_0 = \omega_{pe}$; at a field frequency of 2.45 GHz, n_c corresponds to 7.6×10^{16} m^{-3}. At powers greater than 3 W, n_e is thus above n_c with $n_e > 1 \times 10^{17}$ m^{-3}. It is noteworthy that the power domain near to n_c does not ensure stable calculating conditions, some 'microwave power jumps' possibly occurring when going from below n_c to above n_c values or the other way round. Whether the electron density in figure 11 is below critical density (upper row) or above it (lower row), the electron density is always maximum at the geometrical centre ($y = 0$, $z = 0$) of the discharge tube, and it decreases as both y and z coordinates increase, as would be expected under diffusion conditions owing to the cylindrical symmetry of the discharge tube. Close to the tube walls, on which recombination occurs, the electron density is approximately two orders of magnitude lower than at the geometrical centre.

The set of data for $n_e \leqslant n_c$ is akin to wave propagation in an unbounded plasma ($\omega < \omega_{pe}$) whereas the results for $n_e > n_c$ are, for the time being, tentatively attributed to a bounded wave propagation of the surface-wave type.

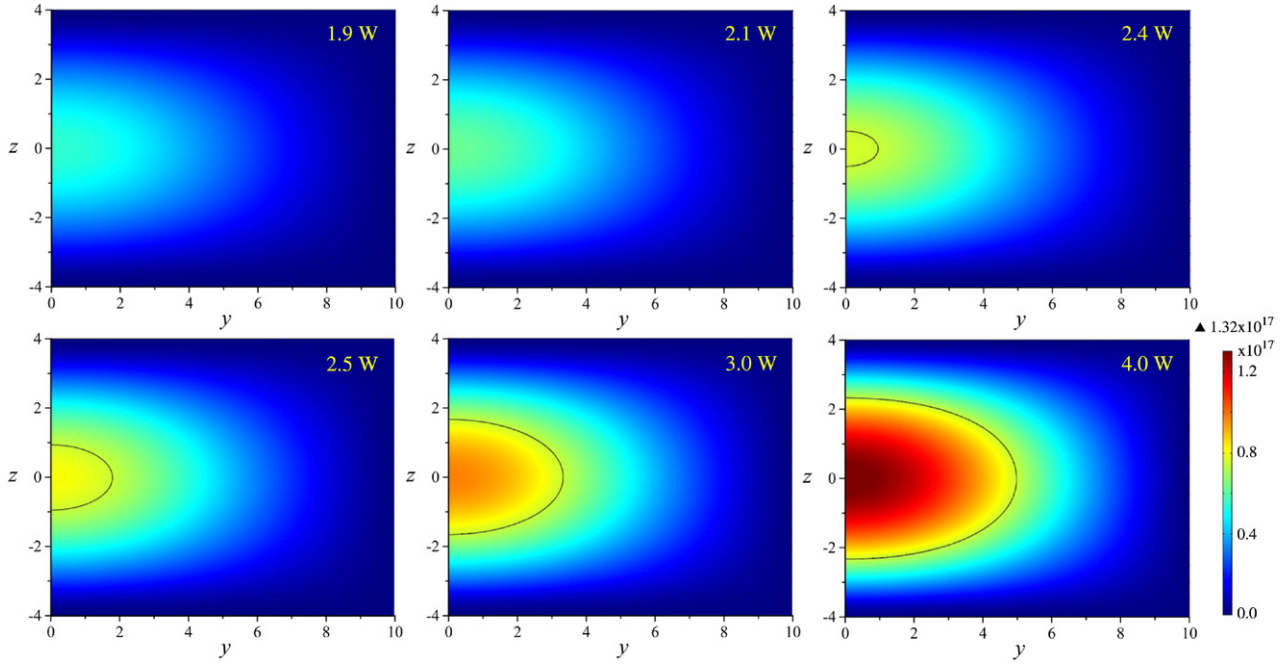

Figure 11. Spatial y and z distributions of electron density (units: m^{-3}) for several values of absorbed power (indicated in the upper right corner of each picture). The black triangle (▲) atop the colour bar indicates the maximum value of electron density actually attained. The electron density is below critical density in the upper row and above it in the lower row: the black line delineates the critical electron density contour.

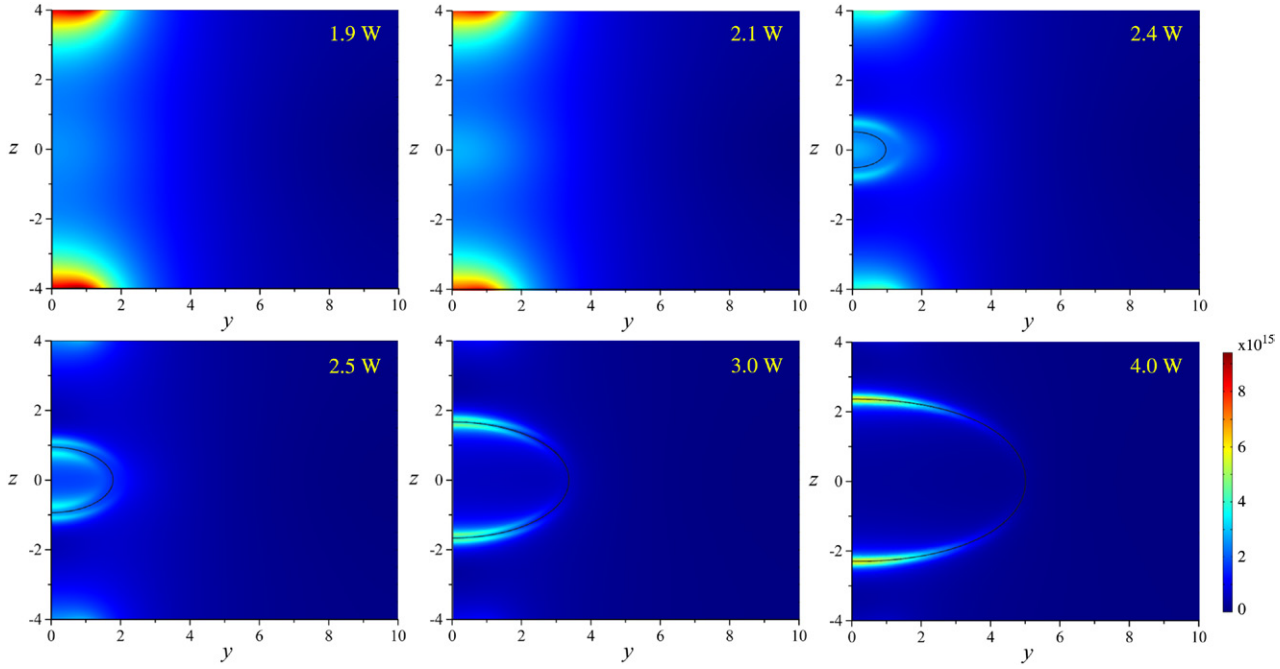

Figure 12. Spatial y and z distributions of the microwave electric field amplitude (units: V m^{-1}) for the same set of absorbed powers as in figure 11. The electron density is below critical density in the upper row pictures and above it in those of the lower row.

5.2. Mapping of the microwave electric field amplitude in the discharge

Figure 12 shows the spatial distribution of the electric field amplitude for the same set of absorbed powers as in figure 11. When microwave power is such that the electron density is below the critical value (recall that the electron density is always maximum close to $y = 0, z = 0$), the electric field intensity is confined to the near vicinity of the antennas, as can be seen from the set of pictures in the upper row in figure 12. In contrast, when n_e exceeds n_c, the intensity of the electric field reaches its maximum in the vicinity of the discharge geometrical centre, more specifically for z in the range -0.5 to 0.5 and for y from 0 to ~1. Such a significant change in the HF electric field configuration following a small variation of the electron density (going from $n_e < n_c$ to $n_e > n_c$) is connected with the well-known fact that at $n_e = n_c$ the real part of the

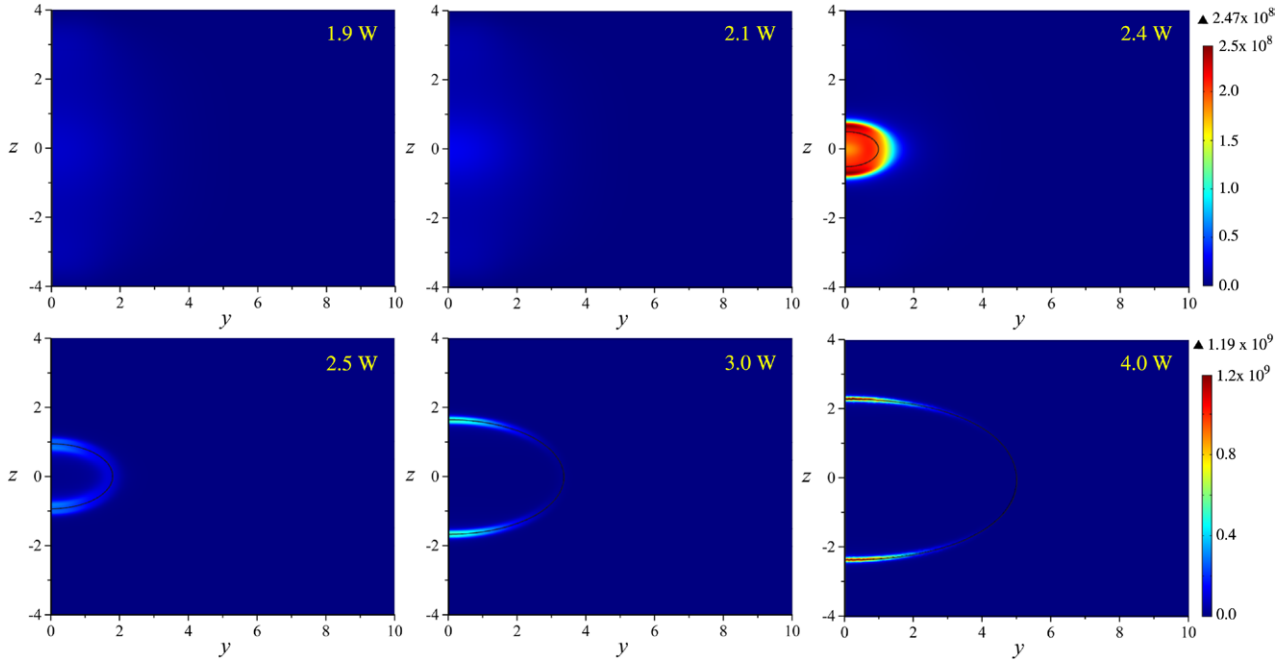

Figure 13. Spatial y and z distributions of the absorbed microwave power (units: W m^{-3}) for the same set of absorbed powers as in figure 11. The electron density is below critical density in the upper row and above it in the lower row. Note that rather high amounts of power density are attained, namely from 10^7 to 10^9 W m^{-3} (10 W cm^{-3} to 1 kW cm^{-3})!

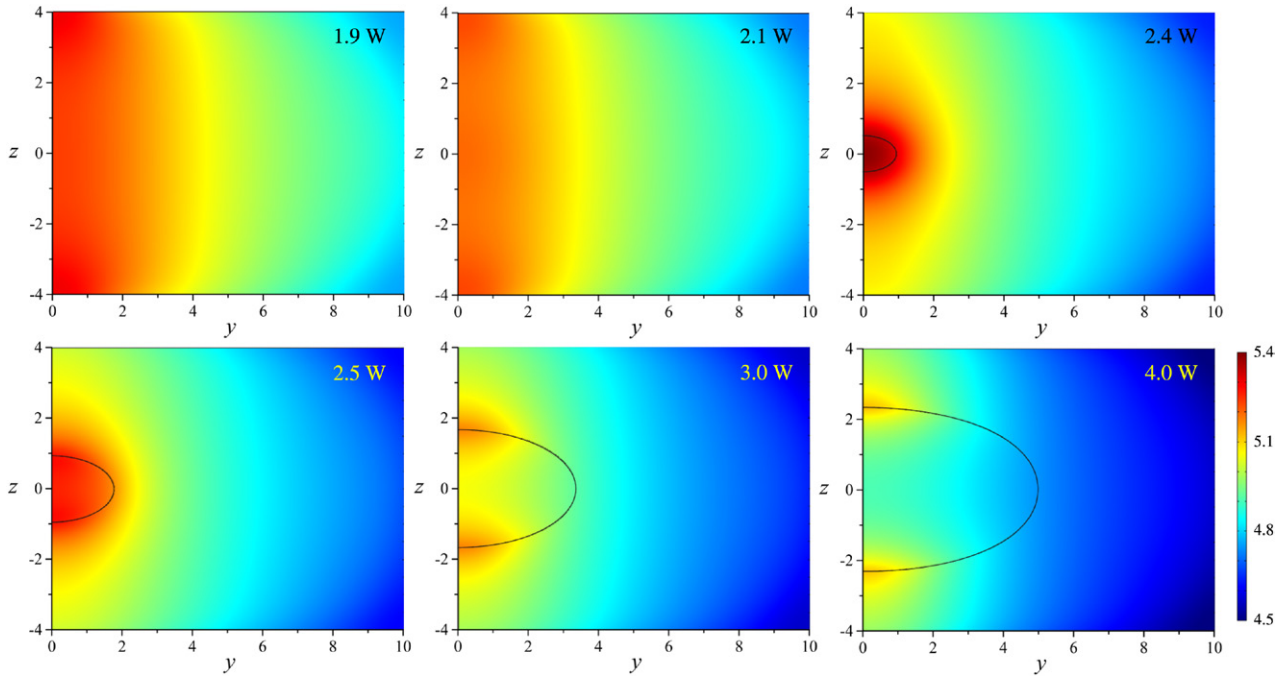

Figure 14. Spatial y and z distributions of the electron temperature (units: eV) for the same set of absorbed powers as in figure 11. The maximum electron density is below critical density in the upper row and above it in the lower row: the black line delineates the critical electron density contour.

complex plasma permittivity passes through zero (see equation (13)).

5.3. Mapping of the absorbed microwave power

The spatial distribution of the absorbed microwave power, which depends on the quantity $Q_{\mathrm{rh}} = 0.5\sigma E_0^2$ (where σ is the electrical conductivity of electrons) appearing in equation (15), is plotted in figure 13 for the same set of absorbed powers as in figure 11. When the maximum value of electron density (which always occurs at the geometrical centre of the system) is below n_{c}, the absorbed power density has its maximum at the geometrical centre of the discharge tube, whereas for absorbed power $\geqslant$2.5 W, the maximum of absorbed power density is at the symmetry axis near the region where $n_{\mathrm{e}} = n_{\mathrm{c}}$. Despite the fact that the spatial distribution of power density is highly non-uniform and follows

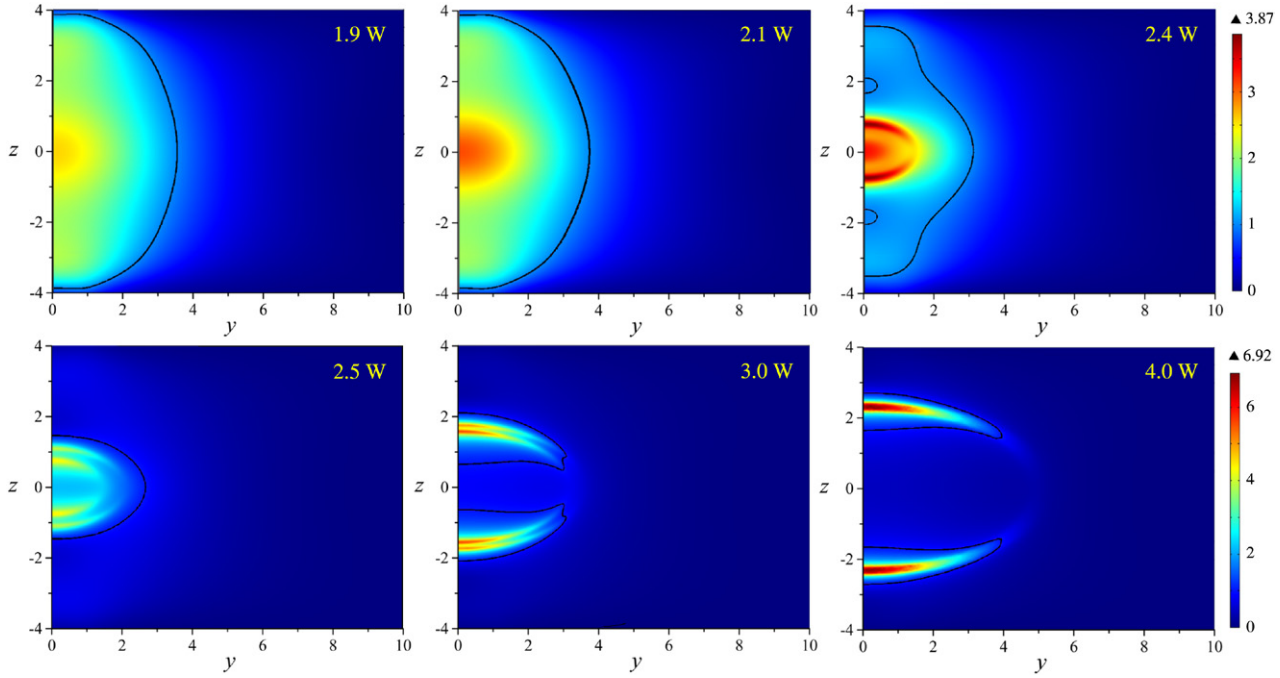

Figure 15. Spatial y and z distributions of the x/λ_{De} ratio (no units) for the same set of absorbed powers as in figure 11. The electron density is below critical density in the upper row and above it in the lower row. The black line indicates the $x/\lambda_{De} = 1$ ratio.

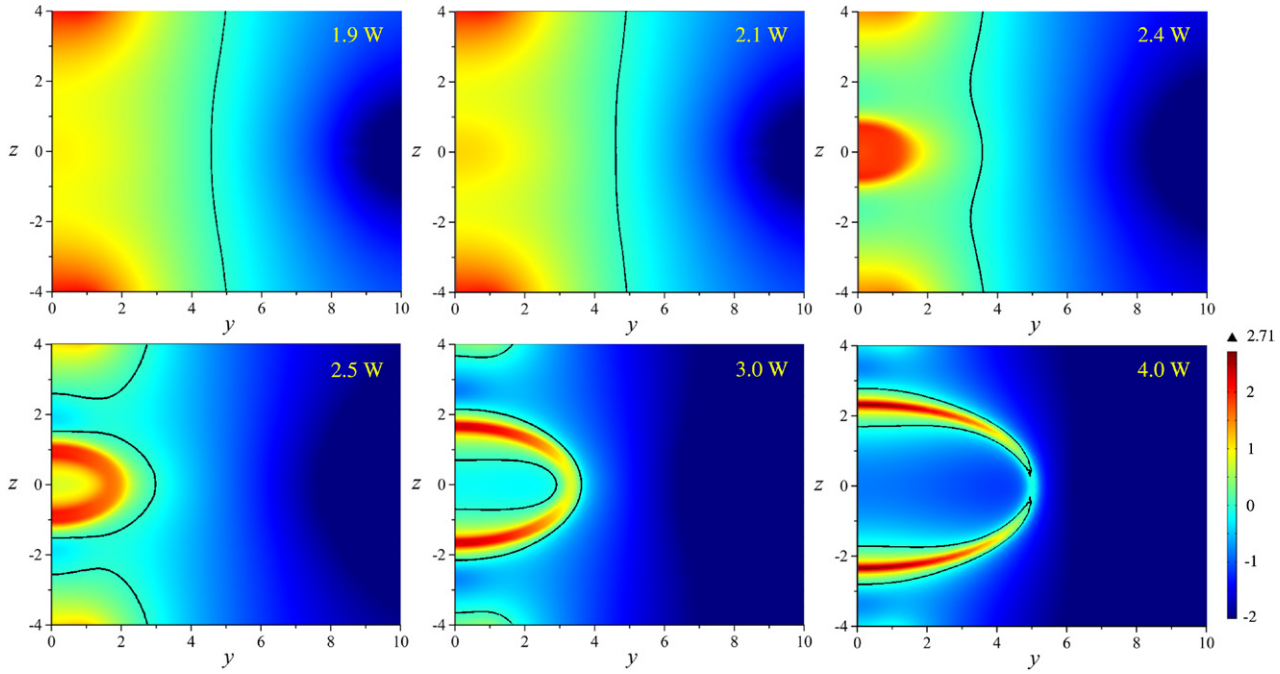

Figure 16. Spatial y and z distributions of the $\log_{10}$ of the (θ_A/θ_L) ratio (no units) for the same set of absorbed powers as in figure 11. The electron density is below critical density in the upper row and above it in the lower row. The black line indicates the $\log_{10}(\theta_A/\theta_L) = 0$ location(s).

different patterns below and above critical density, the electron density distribution nonetheless adopts a similar shape in all cases (figure 11); this is because it is being controlled by diffusion.

5.4. Mapping of the electron temperature

The spatial distribution of the electron temperature T_e is plotted in figure 14 for the same set of absorbed powers as in figure 11. Below critical electron density (upper row), T_e is rather spatially uniform along the z coordinate, as expected under diffusion conditions. In contrast, for an electron density above critical density (lower row pictures), there is a maximum of T_e on both sides of the discharge tube axis, this maximum being located close to the spatial position of the maximum value of the microwave electric field intensity (figure 13). Once again, the rightmost picture in the upper row

(2.4 W) and the leftmost top one in the lower row (2.5 W) can be viewed as a smooth transition from slightly under critical electron density to slightly above it. The value of T_e is in the range 5.1–5.4 eV in the specific configuration examined, whereas in a classical cylindrical discharge for a 6 mm inside diameter tube filled with argon at a gas pressure of 100 mtorr (13.3 Pa) one would get around 3.6 eV.

5.5. Mapping of the x/λ_{De} ratio

Figure 15 displays the spatial distribution of the ratio of the electron amplitude to the electron Debye length. To a first approximation, it is similar to the spatial distribution of the microwave electric field intensity. The maximum (local) value of x/λ_{De} below critical density is in the range 2.6–3.1 while above critical density it is in the range 5.7–6.9 for the power values considered. The higher x/λ_{De} ratios predicted above critical conditions give rise to the so-called Sv periodic parametric emission [3].

5.6. Mapping of the $log10(\theta_A/\theta_L)$ ratio

Figure 16 displays the spatial distribution of the ratio of the power absorbed per electron to the power lost per electron. Below critical density, the maximum (local) value of $\log_{10}(\theta_A/\theta_L)$ is 2.1 and above critical density it is in the range 2.3–2.7. In absolute value, the θ_A/θ_L ratio reaches up locally to a factor of 500! It results from the fact that the volume over which power is absorbed from the microwave field by the electrons is much smaller than that over which this acquired power is lost by collisions with heavy particles. This contrasts with the power balance in a surface wave discharge (section 2.1) where the power absorption and power loss volumes are equal.

6. Summary and perspectives

Using a specific microwave field applicator, we have shown through numerical calculations that the amplitude of the electron in the maintenance E-field is in fact approximately 3–7 times larger than the electron Debye length. Under such conditions, as predicted theoretically by Aliev and Silin's model, the ions are no longer shielded by the electrons and can, therefore, oscillate collectively at their natural frequency, which is the ion-plasma frequency. Such oscillations have in fact been observed [3] and their characteristics fit well within the framework of periodic parametric instabilities under high-intensity EM fields. Such periodic oscillations are limited, in the present case, to pressures below 500 mtorr, one reason being that the amplitude of the electron motion in the HF field loses its meaning under high enough collisions of electrons with heavy species. Specifically, the collision frequency should be low enough so that $\nu \ll \omega_0 \approx \omega_{pe}$ for the E-field to ensure the collective movement of electrons.

We have therefore shown that it is possible, under ambipolar diffusion conditions, to increase the intensity of the electric field sustaining a discharge. This result is based on a power balance analysis involving two physically meaningful parameters: the power lost per electron θ_L and the power absorbed per electron θ_A, and the fact that θ_A adjusts to compensate for losses expressed through θ_L. Practically speaking, it requires that the volume into which power is absorbed from the microwave E-field by the electrons be smaller than that in which this acquired power is lost through collisions of electrons with heavy particles, which then leads to $\theta_A > \theta_L$. In such a situation, the intensity of the maintenance E-field is higher, for instance, than in the case where both these volumes are equal. A corollary feature is that such high-intensity E-fields are generated in non-uniform plasmas.

The calculations presented in the current paper were performed for a low-pressure discharge under ambipolar diffusion, and clearly cannot be extended, as such, to atmospheric pressure discharges, for example. However, one important point emerges from this work: the intensity of the maintenance E-field of a discharge can be increased provided one can modify the degree of non-uniformity of the discharge, such that the volume into which power is absorbed is smaller than the volume in which particles are lost. This assertion can be considered as a general concept applicable to all kinds of plasmas, provided the conditions mentioned above as to the non-uniformity of the discharge are observed.

The current analysis could therefore be employed as a new approach to the investigation of the properties of micro-discharges, which are known to provide a higher level of excitation of atoms and larger degrees of ionization than usual larger-volume discharges. In some of these discharges, the volume over which plasma is generated is so small that it corresponds to a deposited power density that can in fact reach kW cm^{-3}. The size of the volume in which particles are lost compared to the power transfer volume should then be investigated as a starting point.

Acknowledgments

The authors are indebted to Prof Dr A Shivarova and Dr D Kéroack for their precious assistance and comments during the preparation of the manuscript.

References

[1] Moisan M and Pelletier J 2012 *Physics of Collisional Plasmas* (New York: Springer)
[2] Moisan M and Pelletier J 2014 *Plasmas Collisionnels* (Ulis: EDP Sciences)
[3] Moisan M and Leprince P 1975 *Beiträge Plasmaphysik* **15** 83–104
[4] Aliev Y M and Silin V P 1965 *Sov. Phys.—JETP* **21** 601
[5] Porkolab M and Chang R P H 1978 *Rev. Mod. Phys.* **50** 745–95
[6] Drake J F *et al* 1974 *Phys. Fluids* **17** 778–85
[7] Aihara S *et al* 1974 *Plasma Phys. Control. Fusion* **16** 717
[8] Ferreira C M and Moisan M 1988 *Phys. Scr.* **38** 382–99
[9] COMSOL 2010 *COMSOL Plasma Module User's Guide Version 4.1* (COMSOL AB, Sweden)
[10] Lieberman M A and Lichtenberg A J 2005 *Principles of Plasma Discharges and Materials Processing* (New York: Wiley)
[11] Lee I, Graves D B and Lieberman M A 2008 *Plasma Sources Sci. Technol.* **17** 015018
[12] Gregório J *et al* 2012 *Plasma Sources Sci. Technol.* **21** 015013

[13] Koleva I *et al* 2004 *Contrib. Plasma Phys.* **44** 552–7
[14] Makasheva K and Shivarova A 2001 *Phys. Plasmas* **8** 836–45
[15] Hagelaar G J M and Pitchford L C 2005 *Plasma Sources Sci. Technol.* **14** 722
[16] 2014 Phelps database www.lxcat.net (retrieved on July 4 2014)
[17] Lymberopoulos D P and Economou D J 1993 *J. Appl.Phys.* **73** 3668–79
[18] Rafatov I, Bogdanov E A and Kudryavtsev A A 2011 On the numerical modelling of a dc driven glow discharge plasma *30th ICPIG* (*Belfast, 2011*)
[19] Paunska T, Shivarova A and Tarnev K 2011 Comments on the boundary conditions for metal and dielectric walls in the fluid-plasma modelling *30th ICPIG* (*Belfast, 2011*)
[20] Hagelaar G J M et al 2009 *J. Phys.* D **42** 194019